Two-dimensional magnetic correlation and transport behavior of layered manganite $La_{1.4}Sr_{1.6}Mn_{2-x}Cu_xO_7$

Hong Zhu, XiaoJun Xu, Li Pi, and YuHeng Zhang
Structure Research Laboratory, University of Science and Technology of China, Hefei 230026, People's Republic of China
(Received 1 February 2000)

The effect of Cu substitution for Mn in layered manganese oxides $La_{1.4}Sr_{1.6}Mn_{2-x}Cu_xO_7$ on magnetic and transport properties has been investigated. It is interesting that the undoped samples undergo complex transitions with lowing temperature. They transform from the paramagnetic state to the two-dimensional (2D) short-range ferromagnetic (FM) order at ~370 K and then enter the three-dimensional (3D) long-range ferromagnetic state at $T_C \sim 100$ K. At last, they display the metastable canted antiferromagnetic (AF) state and semiconductor behavior below $T_N \sim 50$ K. It is suggested that the semiconductor behavior is correlated to the coexistence of the FM order and the canted AF order below T_N. With increasing Cu doping level, the 3D long range FM order and then the 2D short range correlation disappears in turn and the conduction at $T > T_C$ transforms from the near-neighbor hopping process to the variable-range hopping process.

I. INTRODUCTION

Since the end of the past decade, there has been renewed interest in the mixed-valence $3d$ transition-metal oxides with the perovskite structures because of their strong electron correlation. After the discovery of high-T_c superconductivity (HTSC) in the layered copper oxides,[1] the colossal magnetoresistance (CMR) of the doped manganite perovskites $T_{1-x}D_xMnO_3$ (T=trivalent lanthanide cation, La; D =divalent alkaline-earth cation, Ca, Sr, Ba) with the ABO_3 structure has been the majority of studies in recent years.[2–7] The mixed valence in the Mn ions caused by D^{2+} substitution for T^{3+} creates anomalous transport property and CMR behavior. The basis for the theoretical understanding of the doped manganese oxides is traditionally the notion of double exchange (DE),[8] which considers the exchange of electrons between neighboring Mn^{3+} and Mn^{4+} sites with strong on-site Hund's coupling. But some calculation showed that DE mechanism alone could not explain the experimental data of the Mn oxides, and suggested that a strong Jahn-Teller distortion should be responsible for the transport properties.[9] Despite some effects[10–12] that have included the strong Jahn-Teller type interaction between electrons and lattice, this theory still needs to be refined to account for the large magnetoresistance observed in experiments. Contrary to the above approaches, the localization effect in the DE model[13,14] and a localization model comprising spin disorder and nonmagnetic radomness[15] were suggested later to account for magnetotransport properties in Mn oxides $T_{1-x}D_xMnO_3$.

It is well known that there are many variations of perovskite oxide compound with the general formula $(AO)\times(ABO_3)_n$ (A=lanthanide cation; B=transition metal cation). For copper oxide superconductors, the transition temperature T_c rises with increasing the numbers of CuO_2 layers. So far, the manganese oxide for $n=1$, $La_{1-x}Sr_{1+x}MnO_4$ with a layered perovskite structure (K_2NiF_4 type), has been found to be an insulator without ferromagnetic (FM) phase.[16–18] Recently, magnetoresistance effect and FM transition also have been observed in the manganese oxide for $n=2$, $(La,D)_3Mn_2O_7$ (D=Sr, Ca) with a tetragonal $Sr_3Ti_2O_7$-type bilayered perovskite structure.[6,19–23] The $(La,D)_3Mn_2O_7$ (D=Sr, Ca) perovskite compound with layered structure consists of the MnO_2 bilayers which are respectively separated by the rock-salt-type $(La,D)_2O_2$ layers along c axis.[24] Because of its structural anisotropy, it must presents the anisotropy of physical properties, including magnetic property and transport behavior.[6,22,25] It has been found that the exchange interaction between the Mn t_{2g} core spins in the a-b plane J^{ab} is at least an order of magnitude stronger than that along the c axis J^c.[26] Similarly, the resistivity along c axis is about 2 orders of magnitude greater than that in the a-b plane.[19] In addition, it will provide new interesting physics due to its quasi-two-dimensional character. A recent magnetic neutron scattering measurement on $La_{1.2}Sr_{1.8}Mn_2O_7$ has provided evidence for the coexistence of ferromagnetic (FM) fluctuations between the Mn ions within a single bilayer and more persistent antiferromagnetic (AF) clusters above the Curie temperature T_C.[26] Here the magnetic correlations are two-dimensional (2D) and in short-range. We believed this complex short-range magnetic order within the clusters must influence the transport behavior of layered manganese oxides. The relationship between the 2D magnetic correlation and electrical property need to be clarified. Moreover, we noticed that the p-d orbit hybridization causes antiferromagnetic correlation in CuO_2 layer of the HTSC copper oxide, so the Cu substitution for Mn must suppress the double exchange (DE) interaction between the Mn^{3+} and Mn^{4+} ions. In order to investigate the effect of 2D short range magnetic order to the transport properties above T_C and that of the Cu substitution for Mn, we report the magnetic and electrical measurement on the $La_{1.4}Sr_{1.6}Mn_{2-x}Cu_xO_7$ compounds in this paper. It is found that the systems display the semiconductive behavior at temperature below T_C.

II. EXPERIMENTS

The polycrystalline samples of $La_{1.4}Sr_{1.6}Mn_{2-x}Cu_xO_7$ (x =0.00, 0.05, 0.10, and 0.40) were synthesized by standard

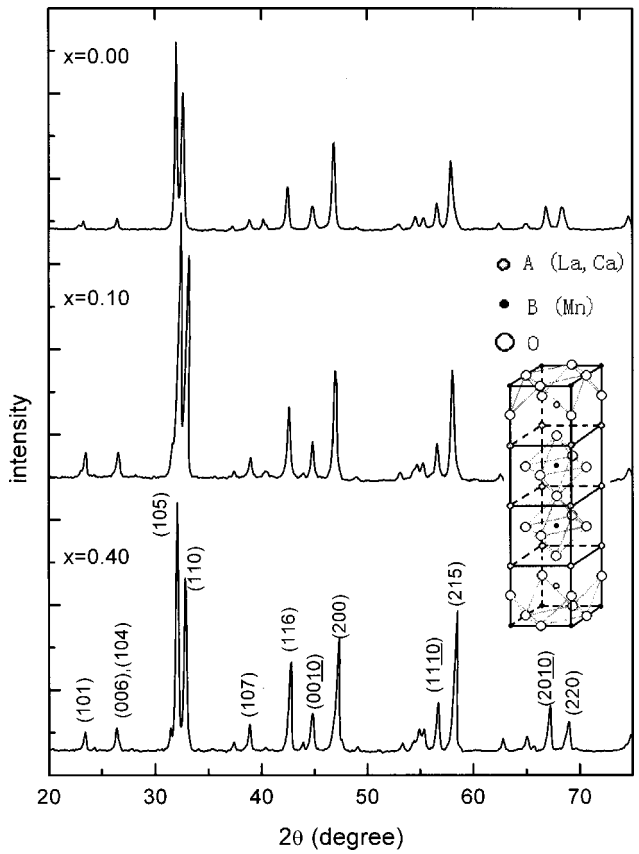

FIG. 1. X-ray diffraction patterns of samples $La_{1.4}Sr_{1.6}Mn_{2-x}Cu_xO_7$.

ceramic technique. The precursor materials were prepared by mixing stoichiometric amounts of CuO, $SrCO_3$, MnO_2, and La_2O_3 that were completely dried prior to use. The powder was ground and calcined at 1000 °C and 1340 °C in air with intermediate grinding. At last it was pressed into ϕ 10 mm plates which were sintered at 1380 °C for 20 h.

To characterize the samples, the x-ray diffraction (XRD) was carried out with Rigaku $D/\mathrm{Max}\text{-}\gamma A$ diffractometer operated with graphite monochromator and using Cu K_α radiation ($\lambda = 0.1542$ nm). The electrical resistivity was measured by standard four-probe method. The measurements were performed as function of temperature from 20 to 350 K. The temperature dependence of magnetization was measured at low field (20 Oe) and high field (10 kOe) on a VSM-9300 vibrating sample magnetometer. In order to investigate the specificity of the paramagnetic state and the short-range magnetic order, we observed the electron spin resonance (ESR) spectra. The ESR measurements were performed using a Bruker ER-200D-SRC spectrometer, operating at 9.47 GHz and between 100 and 300 K.

III. EXPERIMENTAL RESULTS AND DISCUSSION

A. Structure of samples with Cu substitution for Mn site

The x-ray-powder diffraction patterns for samples of $La_{1.4}Sr_{1.6}Mn_{2-x}Cu_xO_7$ ($x = 0.00$, 0.10, and 0.40) are presented in Fig. 1. All the diffraction peaks are indexed with respect to the $Sr_3Ti_2O_7$-type perovskite. The space group is 14/mmm with the lattice parameters of the tetragonal unit cell being $a = 0.387$ nm and $c = 2.021$ nm. The good agreement between the calculated positions of diffraction peaks and the experimental data indicates that the samples are single phases with the $Sr_3Ti_2O_7$-type structure.[6] It is well known that the radius of Cu^{2+}(0.070 nm) and Cu^{3+}(0.068 nm) are very close to that of Mn^{3+}(0.066 nm) and Mn^{4+}(0.060 nm), but they are quite different with that of La^{3+}(0.106 nm) and Sr^{2+}(0.112 nm). So the Cu substitution for La(Sr) must change the lattice parameters obviously under such heavy doping level. Here the little change in the positions of diffraction peaks for heavily doped sample ($x = 0.40$) indicates that Cu ions surely substitute for Mn sites.

As illustrated in the inset of Fig. 1, the crystal structure of $(La,D)_3Mn_2O_7$ ($D = \mathrm{Sr, Ca}$) consists of a two-dimensional network of MnO_6 octahedra. Alternate perovskite bilayers along the c axis are misaligned with respect to each other. Thus the exchange interactions between the Mn ions in the a-b planes and along the c-axis must be different. The magnetic and transport behaviors seem to be two-dimensional or quasi-two-dimensional.

B. Suppression of FM order by Cu doping

The temperature dependence of the electrical resistivity ρ and magnetization M in low (20 Oe) and high (1 kOe) magnetic fields are presented in Fig. 2. All these data were taken in the warming run after zero-field cooling. It can be seen in Fig. 2(a) that for undoped and lightly doped samples ($x \leqslant 0.05$) the ρ-T curves display maximums at higher temperature near 100 K and minimums at lower temperature. For $x = 0.10$, an inflection point appears at temperature near 60 K. With increasing doping level to $x = 0.40$, the transport behavior displays insulatorlike character distinctly. Figures 2(b) and 2(c) display $M \sim T$ curves under low and high magnetic fields, respectively. For an undoped sample ($x = 0.00$), Fig. 2(b) shows that the increase of the M around $\sim$370 K marks the transition from paramagnetic (PM) state to magnetic order state. A visible plateau in low field $M(T)$ curve between 100 K and 370 K shows the short-range 2D FM orders in this temperature range.[26] The magnetization at either fields increase sharply at $T_c \sim 100$ K, which is the signature of the transition from 2D to 3D ferromagnetic (FM) order. The saturation magnetization ($M \sim 60$ emu/g) is the same order as the ferromagnetically ordered $Pr_{1-x}Ca_xMnO_3$,[27] which indicates that the low-temperature phase is ferromagnetic (FM).

Figures 2(b) and 2(c) also show the M-T curves for samples with the different levels of Cu doping under 50 Oe and 10 kOe magnetic fields, respectively. For a low doped sample ($x = 0.00, 0.05$), the 3D FM order is first suppressed by doping and the T_C shifts to low temperature as shown in the inset of Fig. 2(b) and Fig. 2(c). As x increases to 0.10, the 3D magnetic order disappears but the 2D short-range order remains to low temperature. For further doping, the sample with $x = 0.40$ does not display obvious magnetic transition in the measuring temperature range and maintains in the paramagnetic state.

In Fig. 2(b), the reduction of the magnetization at lower temperature for undoped sample indicates an antiferromagnetic (AF)-type transition at temperature $\sim$60 K which is defined as Neel temperature T_N. The neutron scattering has

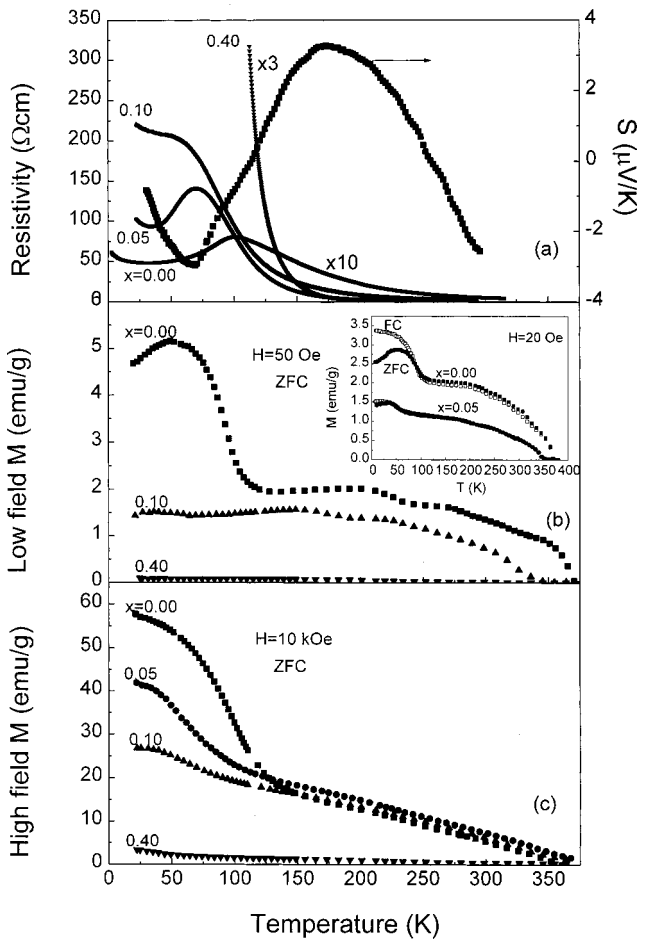

FIG. 2. Temperature dependence of (a) electrical resistivity, (b) low field magnetization, and (c) high field magnetization for samples $La_{1.4}Sr_{1.6}Mn_{2-x}Cu_xO_7$. The Seaback coefficient S for undoped sample ($x=0.00$) also shown as a function of temperature in (a). Inset: comparison of M vs T between field cooling (FC) and zero field cooling (ZFC).

indicated that the interlayer canted antiferromagnetic (AF) order takes place and evolves below T_N.[26,28,29] To clarify this AF transition, we measured the temperature dependence of low field magnetization in both zero field cooling (ZFC) and field cooling (FC) as shown in the inset of Fig. 2(b). Above T_C, the ZFC magnetization is the same as the FC magnetization. It is noteworthy that the temperature dependence of magnetization in the two cooled conditions is quite different below $T_N \sim 60$ K. The ZFC magnetization decreases with decreasing temperature. However, the FC magnetization just exhibits FM behavior. The λ type transition in low field $M \sim T$ curve implies that the spin-glass transition occurs near T_C for undoped and lightly doped samples ($x \leqslant 0.05$). In ZFC condition, this canted AF arrangement between the adjacent bilayers is frozen up at low temperature. During measurement, the external field forces parts of the antiparallel spins trending towards the direction of field and the parallel spins align more collinear. So the measured magnetization is greater than that under zero field. With increasing temperature, the antiparallel spins have more chances to flip toward the external field by the thermal fluctuation and the magnetization increases. In FC condition, the spins align and are frozen up parallel to the field because the transition from PM to FM state occurs in the external field. So that the magnetization does not decrease below T_N.

In order to investigate the specificity of the short-range magnetic order in the temperature range 100–300 K, we measured the ESR spectra for different doping samples. The asymmetry, complex signals with g value much greater than 2 are observed in the differential spectra $dP/dH-H$, as shown in Fig. 3. To analyze these complicated spectra, we integrate $dP/dH-H$ and get the absorption curve P-H which is fitted quite well by the two Lorentzian lines. Figure 4 shows the absorption curves and their fitting results. The two ESR peaks indicate that there are two kinds of resonance in these systems. This is in contrast with the pseudocubic manganite perovskites $T_{1-x}D_xMnO_3$, where only one paramagnetic ESR line with $g \sim 2.0$ is presented for $T > T_C$. For undoped sample, the two lines deviate from paramagnetic absorption position corresponding $g \sim 2.0$ and shift to low field with cooling as shown in Fig. 4(a). This is the result of antiferromagnetic (AF) correlation and 2D short-range ferromagnetic (FM) fluctuations above T_C. The low field lines are associated with the ferromagnetic microdomains, in which the spins parallel to external field. The high field lines are associated with the antiferromagnetic microdomains. For the sample with $x=0.10$, the two resonance lines shift to high field comparing with the undoped sample. For $x=0.40$

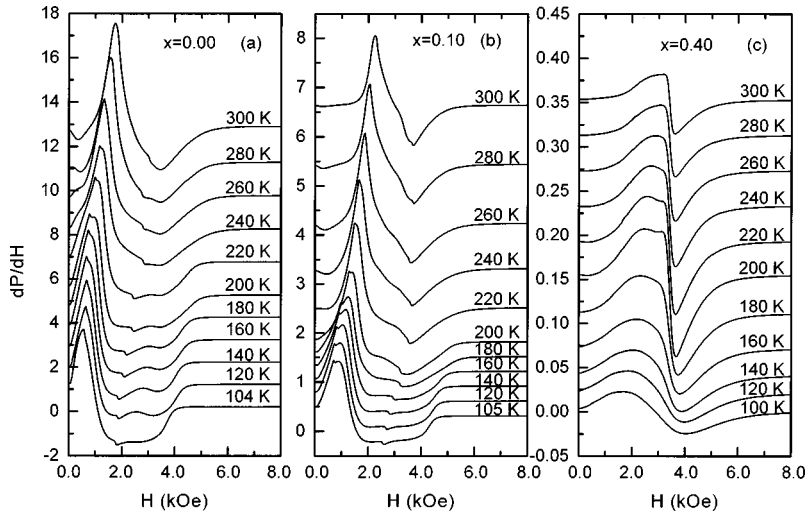

FIG. 3. X-band, 9.47 GHz ESR spectra of samples $La_{1.4}Sr_{1.6}Mn_{2-x}Cu_xO_7$ ($x=0.00$, 0.10, and 0.40) taken at different temperatures for $100\ \text{K} < T < 300\ \text{K}$.

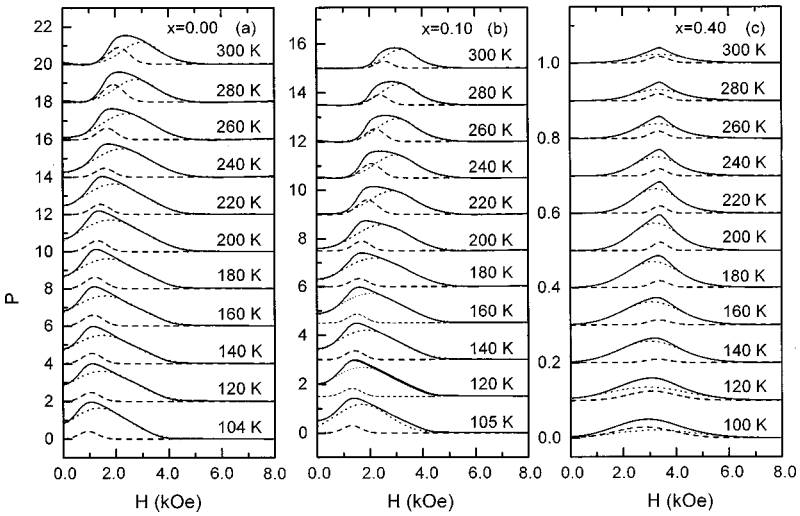

FIG. 4. The absorption curves $P \sim H$ obtained by integration of ESR spectra of samples $La_{1.4}Sr_{1.6}Mn_{2-x}Cu_xO_7$ at different temperatures. The dashed lines show the high field and low field components.

(Mn ions decrease for ~20%), the absorption intensity is smaller for 2 orders than that of undoped sample; moreover, the low field lines stay at the paramagnetic absorption position corresponding $g \sim 2.0$ until $T \sim 140$ K and the high field line shift to low field below 200 K as shown in Fig. 4(c). This is in agreement with the *M-T* curve in Figs. 2(b) and 2(c) for $x = 0.40$. For heavily doped sample ($x = 0.40$), the magnetic correlation microdomains are smaller, so that the double exchange interaction between the Mn ions is destroyed seriously and no FM order occurs in the whole temperature range. The result suggests that the Mn^{3+}-O-Mn^{4+} microdomains cannot form in heavily doped samples and e_g electrons are localized at Mn^{3+} sites. So the system is in paramagnetic state and its electrical resistivity exhibits the insulatorlike behavior as shown in Fig. 1(a).

As x decreases to 0.10, the Mn^{3+}-O-Mn^{4+} microdomains are bigger and they would enter FM state separately at the temperature corresponding 2D short-range order state. The ESR lines corresponding to FM microdomains occur below $T \sim 280$ K. The PM lines only appear above 280 K as shown in Fig. 4(b). This means that the DE interaction within the clusters overcomes the thermal fluctuation, so that the ESR lines shift to low field and the resonance lines corresponding to the FM order appear. It can be seen in Fig. 4 that with x increasing, the high field lines shift to PM absorption position. This indicates that not only the magnetic coupling between the bilayers but also the AF coupling within the layers are suppressed under 3400 Oe field. So the correlations between the Mn ions decrease and disappear. Therefore the systems enter paramagnetic states.

It is well known in the double exchange (DE) model that the hopping of e_g electrons between Mn ions via O^{2-} ions causes the parallel alignment of Mn t_{2g} core spins.[22] The Cu substitution for Mn creates Cu-O-Mn bonds. In HTSC compounds, the superexchange interaction through *p-d* σ orbit hybridization causes the AF arrangement of the spins in the Cu ions. Therefore AF correlation in Cu-doped CMR manganite suppresses DE interaction between Mn ions and destroys FM microdomains within MnO_2 bilayers. The e_g electrons are localized in the Mn^{3+} ions and the core spins of Mn ions are not correlated, so that the 2D short-range order occurs in clusters which are arranged in disorder by doping. And in the heavily doped samples, such as for $x = 0.40$, the cluster is too small to form the short-range FM order and the paramagnetic behavior presents in the whole measuring temperature range.

C. Polaron hopping conductivity at $T > T_C$

The temperature dependence of electrical resistivity ρ for samples with different doping levels is shown in Fig. 2(a). The resistivities increase obviously with increasing of Cu doping. For the undoped sample ($x = 0.00$), the peak near $T^{\rho}_{max} \sim 100$ K in the ρ-T curve indicates that the sample passes through the metal-insulator (MI) transition. At temperatures above T^{ρ}_{max} the resistivity increases with decreasing temperature ($d\rho/dT < 0$) as the semiconductorlike behavior. But below T^{ρ}_{max} the resistivity decreases, then increases after reaching the minimum value. The marked minimum is presented at $T^{\rho}_{min} \sim 40$ K for the undoped sample ($x = 0.00$). As the Cu doping is light ($x = 0.05$), the main behavior of the resistivity is similar to that of undoped sample. Besides increasing for an order, the peak in the ρ-T curve, signal of the *M-I* transition, shifts to low temperature as shown in Fig. 2(a), but it can be seen that the temperature corresponding to the minimum is not affected greatly by Cu doping. For $x = 0.10$, no metallic behavior appears but the inflection point at 60–40 K is presented in ρ-T curve. The resistivity of the heavily doped sample ($x = 0.40$) behaves like insulator in the whole measuring temperature range. This is in agreement with the disappearance of the magnetic correlation.

As mentioned above, the 2D short-range magnetic order occurs in ab plane above Curie temperature T_C. In order to clarify its influence to transport property, we analyze the ρ-T curves carefully as shown in Fig. 5. Both the Arrhenius law[30] $\rho = \rho_0 \exp(E_\rho/kT)$ and the nearest-neighbor hopping[31] of polarons $\rho = AT \exp(W_P/kT)$ fit the experimental data quite well above $T \sim 200$ K and give $E_\rho = 114$ meV, $W_P = 109$ meV respectively. But it is difficult to distinguish between the two models. It is well known that thermoelectric power can supply the useful information about the transport properties. In order to identify the dominant conductive mechanism, we measured the temperature dependence of the thermoelectric power for undoped sample. In the band-gap model of semiconductor, the activated energy E_ρ is equal to the characteristic energy E_S of the thermoelectric power

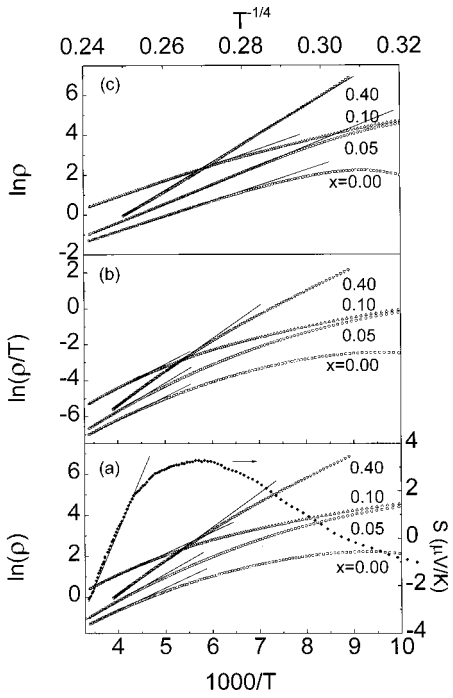

FIG. 5. (a) $\ln(\rho)$ and (b) $\ln(\rho/T)$ shown as a function of inverse temperature (bottom axis) for samples $La_{1.4}Sr_{1.6}Mn_{2-x}Cu_xO_7$. The Arrhenius law and nearest-hopping models fit the data in a narrow temperature range. (c) $\ln(\rho)$ as a function of $T^{-1/4}$ (top axis) for the samples. The variable-range hopping model fits the data in a wider temperature range. The temperature dependence of S for undoped sample is also shown in (a) (right axis).

which is given by expression: $S=(k/e)(E_S/kT)+S_\infty$, where S is the Seaback coefficient.[32] When the characteristic energy E_S is much lower than E_ρ, it is considered that the hopping process of polaron dominates the conduction.[33] At $T>200$ K our thermoelectric power data is fitted quite well by the linear relation between S and $1/T$ and its slope gives $E_S=5.0$ meV as shown in Fig. 5(a). The E_S is much lower than the activated energy $E_\rho=114$ meV given by $\ln(\rho)\sim T$ curve. Therefore we suggest that the hopping process of polaron, excluding the conventional band transport, dominates the conductivity of the system. Accompanying with short range FM order in the temperature range $T_C<T<370$ K as the results of magnetic measurement mentioned above, the polarons are the e_g electrons coupling with FM clusters, so that the activated energy E_ρ is quite great here.

So far many experiments have provided the evidences for the hopping conduction in doped manganese oxides at $T>T_C$. The two hopping models, the nearest-neighbor hopping[31] and the variable-range hopping,[34] have been reported. But which one is the intrinsic mechanism is not clear. Therefore we give the $\ln\rho$ as a function of $T^{-1/4}$ in Fig. 5(c). The solid line is the fiting curve for the variable-range hopping (VRH) model. The polaron $\rho=AT\exp(W_p/kT)$ and the VRH formulas $\rho=\rho_\infty\exp[(T_0/T)^{1/4}]$ are used to fit the data of the resistivity respectively. The fitting parameters are given in Table I. For undoped sample, both of the hopping models (the near-neighbor and the variable-range) are adaptable but it is difficult to say which one is more favorable at $T>200$ K. For the Cu substitution for Mn, the VRH model fits the data well in wider temperature range ($T>150$ K) than the near-neighbor hopping model does ($T>240$ K). The transition of the two hopping processes is mostly lied on relation between the localization length $1/\alpha$ and the average distance of nearest localized state R_0.[33] When $R_0\gg 1/\alpha$, the conduction is favorable for near-neighbor hopping process. When $R_0\leqslant 1/\alpha$, it is the VRH process. For undoped sample, R_0 and $1/\alpha$ are almost in the same order ($R_0\sim 1/\alpha$), it is difficult to distinguish the two models. For lightly doped sample ($x=0.05$), the distribution of random potential field creates a lot of new localized states and the R_0 decreases. As $R_0\leqslant 1/\alpha$, the VRH process dominates the conduction mechanism. In pseudocubic $R_{0.67}D_{0.33}MnO_3$ compounds, the hopping process of the small polaron dominates the transport property above T_C. But in $La_{2-2x}Sr_{1+2x}Mn_2O_7$ system, it seems difficult for the small polaron to form in the background of 2D short-range FM order. It can be seen in Table I that the formation energy W_P of the polaron increases with doping level, this indicates that Cu substitution for Mn is not in favor of the large magnetic polaron and the VRH process is reasonable.

The characteristic temperature T_0 depends on the localization length $1/\alpha$ of the electrons by[35] $T_0=24\alpha^3/\pi g_{(E_F)}k_B$, $g(E_F)$ denotes the density of states at the Fermi level. Using the localization length $1/\alpha\sim 10^{-10}$ m, we deduced that the density of state $g(E_F)\sim 10^{21}$/eV cm^3. The order of $g(E_F)$ is reasonable in physics.

The magnetization plateau from 100 to 370 K and ESR measurement mentioned above show that FM short-range-order takes place reliably at temperature above T_C. The ZFC and FC magnetization measurement indicates that the spin-glass transition occurs at low temperature. The spins are FM ordered in clusters, but they are arranged in disorder between clusters. Such magnetic structure, so called cluster-spin-glass, dominates the transport properties in this temperature range. Here the carriers are the palarons which is the e_e electron coupling with the FM clusters. The degree of disorder between clusters increases with the increase of doping level. For $x=0.40$, the PM signals in ESR patterns indicate

TABLE I. Fitting parameters and valid temperature ranges of the various samples for the polaron and the variable-range hopping VRH model.

x	T range (K)	Polaron W_p (meV)	A (Ω cm/K)	T range (K)	VRH $T_0(10^6$ K)	ρ_∞ (Ω cm)
(0.00)	>210	109	1.2×10^{-5}	>160	16.8	5.2×10^{-8}
(0.05)	>220	131	7.5×10^{-6}	>140	40.0	1.0×10^{-9}
(0.10)	>210	115	5.5×10^{-5}	>170	20.3	1.3×10^{-7}
(0.40)	>175	161	2.5×10^{-6}	>130	187	1.7×10^{-13}

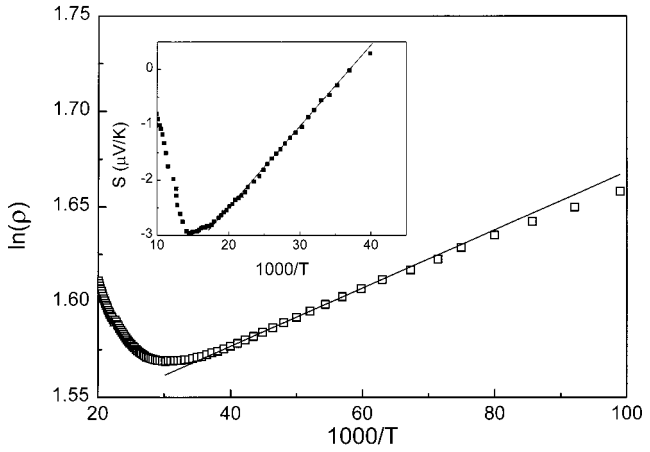

FIG. 6. ln(ρ) at low temperature shown as a function of $1/T$ for undoped sample $La_{1.4}Sr_{1.6}Mn_2O_7$. The solid line is a fit of Arrhenius law to the data. Inset: Seaback coefficient S vs $1/T$.

that with heavily doping the e_g electrons are localized at disordered sites. The VRH transport is favored in the disorder background. So with increasing doping level the transport mechanism changes from near-neighbor hopping process to the VRH process.

D. Semiconductive transport behavior at $T<T_C$

When undoped sample enter 3D FM phase at $T<T_C$, the polarons are delocalized into itinerant electrons and the electrical resistivity decrease sharply. With lowering the temperature further, it is noteworthy that the minimums of the resistivity and the thermoelectric power appear at $T^{\rho}_{\min}$ $\sim$40 K. To clarify the low temperature transport behavior, we have plotted ln(ρ) as the function of $1/T$ at $T<40$ K in Fig. 6. The data is fitted quite well with the linear relation and its slope gives the activation energy $E_\sigma=0.13$ meV. At the same temperature range, its thermoelectric power also meet the semiconductorlike temperature dependence $S=(k_B/e)(E_S/kT)+S_\infty$ and the characteristic energy $E_S=0.11$ meV as shown in the inset of Fig. 6. Here $E_\sigma \approx E_S$, this is the character of the band transport in a typical semiconductor. Hence in contrast with the conductivity at $T>T_C$, the semiconductive transport at low temperature is not due to the hopping process between localized states, but due to the band transport process. In addition, the $S<0$ indicates that the carrier is electron-type in this temperature range.

It is well known that for their parent compounds $RMnO_3$, the core spins of the Mn ions are in AF arrangement at $T<T_N$ and the e_g electrons are localized at Mn sites, so the samples present insulator behavior. But for $R_{1-x}D_xMnO_3$ manganese oxides with divalent alkaline-earth cation doping, the core spines of Mn ions are in FM arrangement with the e_g electrons delocalized into itinerant electrons at $T<T_C$. So that the electrical resistivity decrease sharply and the samples present metallic transport. For layered manganese, the interactions of AF order and FM order in layered manganese at low temperature cause that the systems display semiconductor characters.

IV. CONCLUSIONS

In summary, Mn ions are successfully substituted by Cu ions using solid state reaction method for layered perovskite $La_{1.4}Sr_{1.6}Mn_{2-x}Cu_xO_7$. We have presented results on the magnetic, transport properties. Our results show that for lightly doped samples 2D short-range FM clusters occur above the Curie temperature T_C. The double exchange interactions between the mixed-valent Mn ions are suppressed by Cu doping. As $x=0.10$, the 3D FM order and metal-insulator transition disappears. With increasing Cu doping level, the 2D short-range order disappears subsequently. It is suggested that conductivity above T_C is dominant by the variable-range hopping process. For undoped sample $La_{1.4}Sr_{1.6}Mn_2O_7$, the minimum of resistivity and semiconductive transport behavior appear in low temperature. In contrast to the polaron hopping process at $T>T_C$, the low temperature semiconductor behavior is band transport process and is correlative with the interactions between the interlayer canted AF orders and the entralayer FM orders at $T<T_N$. The anisotropy exchange interaction, which is not occurred in pseudocubic manganese oxides, causes quite different magnetic and transport properties in layered perovskite. The new dimensional effect is worthy of studying in detail.

ACKNOWLEDGMENTS

This work was supported by the National Natural Science Foundation of China, No. 19934003 and the Research Fund for the Doctoral Program of Higher Education. We are very grateful to Dr. Yunhua Xu for the ESR measurement.

[1] J. G. Bednorz and K. A. Z. Muller, Phys. Bl. **64**, 189 (1986).
[2] A. Urushibara, Y. Moritomo, T. Arima, A. Asamitsu, G. Kido, and Y. Tokura, Phys. Rev. B **51**, 14 103 (1995).
[3] P. Schiffer, A. P. Ramirez, W. Bao, and S.-W. Cheong, Phys. Rev. Lett. **75**, 3336 (1995).
[4] P. G. Radaelli, M. Marezio, H. Y. Hwang, S.-W. Cheong, and B. Batlogg, Phys. Rev. B **54**, 8992 (1996).
[5] Y. Moritomo, A. Asamitsu, and Y. Tokura, Phys. Rev. B **56**, 12 190 (1997).
[6] J. F. Michell, D. N. Argyriou, J. D. Jorgensen, D. G. Hinks, C. D. Potter, and S. D. Bader, Phys. Rev. B **55**, 63 (1997).
[7] J. M. De Teresa, M. R. Ibarra, J. Blasco, J. Garcia, C. Marquina, P. A. Algarabel, Z. Arnold, K. Kamenev, C. Ritter, and R. Von Helmholt, Phys. Rev. B **54**, 1187 (1996).
[8] C. Zener, Phys. Rev. **82**, 403 (1951); J. Volger, Physica (Amsterdam) **20**, 49 (1954); P. W. Anderson and H. Hasegawa, Phys. Rev. **100**, 675 (1955); P.-G. DeGennes, *ibid.* **118**, 141 (1960).
[9] A. J. Millis, P. B. Littlewood, and B. I. Shraiman, Phys. Rev. Lett. **74**, 5144 (1995).
[10] A. J. Millis, P. B. Littlewood, and B. I. Shraiman, Phys. Rev. Lett. **77**, 175 (1996); Phys. Rev. B **54**, 5389 (1996); **54**, 5405 (1996).
[11] H. Roder, J. Zang, and A. R. Bishop, Phys. Rev. Lett. **76**, 1356 (1996).

[12] J. D. Lee and B. I. Min, cond-mat/9704051 (unpublished); cond-mat/9704052 (unpublished).
[13] E. Muller-Hartmann and E. Doggoto, Phys. Rev. B **54**, R6819 (1996).
[14] C. M. Varma, Phys. Rev. B **54**, 7328 (1996).
[15] L. Sheng, D. Y. Xing, D. N. Sheng, and C. S. Ting, Phys. Rev. Lett. **79**, 1710 (1997).
[16] Y. Moritomo, Y. Tomioka, A. Asamitsu, Y. Tokura, and Y. Matsui, Phys. Rev. B **51**, 3297 (1995).
[17] B. J. Sternlieb, J. P. Hill, U. C. Wildgruber, G. M. Luke, B. Nachumi, Y. Moritomo, and Y. Tokura, Phys. Rev. Lett. **76**, 2169 (1996).
[18] Y. Murakami, H. Kawada, H. Kawata, M. Tanaka, T. Arima, Y. Moritomo, and Y. Tokura, Phys. Rev. Lett. **80**, 1932 (1998).
[19] Y. Moritomo, Y. Tomioka, A. Asamitsu, Y. Tokura, and Y. Matsui, Nature (London) **380**, 141 (1996).
[20] H. Asano, J. Hayakawa, and M. Matsui, Appl. Phys. Lett. **68**, 3638 (1996).
[21] D. N. Argyriou, J. F. Mitchell, C. D. Potter, S. D. Bader, R. Kleb, and J. D. Jorgensen, Phys. Rev. B **55**, R11 965 (1997).
[22] T. Kimura, Y. Tomioka, H. Kuwahara, A. Asamitsu, M. Tamura, and Y. Tokura, Science **274**, 1698 (1996).
[23] R. Seshadri, A. Maignan, M. Hervieu, N. Nguyen, and B. Raveau, Solid State Commun. **101**, 453 (1997).
[24] S. N. Ruddlesden and P. Poper, Acta Crystallogr. **11**, 54 (1958).
[25] D. N. Argyriou, J. F. Mitchell, J. B. Goodenough, O. Chmaissem, S. Shout, and J. D. Jorgensen, Phys. Rev. Lett. **78**, 1568 (1997).
[26] T. G. Perring, G. Aeppli, Y. Moritomo, and Y. Tokura, Phys. Rev. Lett. **78**, 3197 (1997).
[27] M. R. Lees, J. Barratt, G. Balakrishnan, D. McK. Paul, and C. D. Dewhurst, J. Phys.: Condens. Matter **8**, 2967 (1996).
[28] T. Kimura, A. Asamitsu, Y. Tomioka, and Y. Tokura, Phys. Rev. Lett. **79**, 3720 (1997).
[29] D. N. Argyriou, T. Kelley, J. F. Mitchell, R. A. Robinson, R. Osborn, S. Rozenkrantz, R. I. Sheldon, and J. D. Jorgensen, J. Appl. Phys. **83**, 6374 (1997).
[30] R. M. Kusters, J. Singleton, and D. A. Keen, Physica B **155**, 362 (1989).
[31] G. J. Snyder, R. Hiskes, S. DiCarolis, M. R. Beasley, and T. H. Geballe, Phys. Rev. B **53**, 14 434 (1996).
[32] H. Fritzsche, Solid State Commun. **9**, 1813 (1971).
[33] N. F. Mott and E. A. Davis, *Electronic Processes in Non-Crystalline Materials*, 2nd ed. (Clarendon Press, Oxford, 1979).
[34] M. Viret, L. Ranno, and J. M. D. Coey, Phys. Rev. B **55**, 8067 (1997).
[35] Sir Nevill Mott, *Conduction in Non-Crystalline Materials* (Clarendon Press, Oxford, 1993).